Magnetic Resonance in Medicine 41:793–799 (1999)

# Particle Trace Visualization of Intracardiac Flow Using Time-Resolved 3D Phase Contrast MRI

Lars Wigström,[1]* Tino Ebbers,[2] Anna Fyrenius,[1] Matts Karlsson,[2,3] Jan Engvall,[1] Bengt Wranne,[1] and Ann F. Bolger[4]

**The flow patterns in the human heart are complex and difficult to visualize using conventional two-dimensional (2D) modalities, whether they depict a single velocity component (Doppler echocardiography) or all three components in a few slices (2D phase contrast MRI). To avoid these shortcomings, a temporally resolved 3D phase contrast technique was used to derive data describing the intracardiac velocity fields in normal volunteers. The MRI data were corrected for phase shifts caused by eddy currents and concomitant gradient fields, with improvement in the accuracy of subsequent flow visualizations. Pathlines describing the blood pathways through the heart were generated from the temporally resolved velocity data, starting from user-specified locations and time frames. Flow trajectories were displayed as 3D particle traces, with simultaneous demonstration of morphologic 2D slices. This type of visualization is intuitive and interactive and may extend our understanding of dynamic and previously unrecognized patterns of intracardiac flow. Magn Reson Med 41:793–799, 1999.** © **1999 Wiley-Liss, Inc.**

**Key words: magnetic resonance imaging; three-dimensional visualization; heart; phase correction**

The patterns of flow within the heart are time varying and spatially complex. Vortices of different timing and sizes conserve the momentum of moving blood, avoid abrupt deceleration of flow at the heart walls, and influence the opening and closing of the heart valves (1–4); via these mechanisms they affect the efficiency of cardiac filling and ejection. Intracardiac flows remain poorly defined even in the normal heart, as their three-dimensional (3D) nature has been difficult to describe with 2D methods. Doppler echocardiography combines 2D imaging with angle-sensitive, single velocity component measurements of flow. Echocardiographic data have suggested that flow patterns change with cardiac diseases (5–8) but cannot describe either normal or deranged flow in an accurate or complete manner. 2D phase contrast MRI measures all three velocity components within 2D slices (9–12), but the small number of available slices hinders 3D visualization.

A more complete description of 3D flow patterns can be obtained from MRI using a 3D cine phase contrast sequence (13). This type of acquisition generates a huge amount of data and requires a robust visualization technique to produce useful information. One approach has been to use vector plots similar to those that are used to visualize velocity data from 2D slices (14–16). When applied to a 3D grid, however, the density of the displayed vectors impairs comprehension of the flows that they represent.

Particle trace visualization is a visualization technique often used in computational fluid dynamics (CFD) (17). It simulates the path taken by imaginary particles released at a specified location and at a certain time in the given velocity field. As only the released particles are followed, the amount of information displayed is reduced to a level where it is more easily appreciated. Particle motion can be followed along either streamlines or pathlines. Streamlines, which are based on the velocity field for a single time frame, have been shown to produce an accurate visualization of the instantaneous velocity field (18,19). In contrast, pathlines are calculated from temporally resolved velocity data and are used in this study to incorporate the temporal nature of dynamic intracardiac flow.

## MATERIALS AND METHODS

### Data Acquisition

Phase contrast data describing normal intracardiac flow was acquired from human volunteers using a Signa Horizon Echospeed 1.5 T scanner (GE Medical Systems, Milwaukee, WI), which has a high-performance gradient subsystem with a maximum gradient amplitude of 22 mT/m and a slew rate of 120 T/m/sec. To acquire time-resolved 3D information, a conventional 3D phase contrast pulse sequence was modified to allow off-line retrospective gating (13). The resulting 3D cine pulse sequence was used with the signal from a pulse oximeter device to reconstruct data from multiple phases of the cardiac cycle.

The parameters used with the sequence were as follows: TR 18 msec, TE 6 msec, flip angle 20°, field of view (FOV) 30 × 30 × 12.8 cm, matrix size 256 × 96 × 16, velocity encoding range ± 60 cm/sec. The 3D volume was positioned to encompass the entire heart using axial slices. Velocity-encoded data were acquired in all three directions. With the four necessary echoes interleaved (flow compensated and x, y, z encoded), the resulting sampling interval was 72 msec (4 × TR). Since no k-space segmentation was used, the total scan time for the 3D cine sequence was approximately 29 min.

To acquire data for the complete cardiac cycle, an off-line retrospective gating technique is used (20,21). The acquisition of the four velocity encoded echoes is repeated at least 16 times (16 × 0.072 = 1.15 sec) for each phase-encoding

[1]Department of Clinical Physiology, Linköping University, Linköping, Sweden.

[2]Department of Biomedical Engineering, Linköping University, Linköping, Sweden.

[3]Department of Mechanical Engineering, Linköping University, Linköping, Sweden.

[4]Division of Biomedical Science, University of California at Riverside, Riverside, California.

Grant sponsor: Swedish Medical Research Council; Grant sponsor: the Swedish Heart Lung Foundation; Grant sponsor: Forum Scientum.

*Correspondence to: Lars Wigström, Department of Medicine and Care, Clinical Physiology, Linköping University, S-581 83 Linköping, Sweden.
E-mail: larsw@mr.us.lio.se

Received 19 June 1998; revised 12 October 1998; accepted 13 October 1998.

step, to ensure that data from at least one complete cardiac cycle are collected for every line in k-space. Additional samples falling outside the first heart cycle are wrapped back into the first beat to improve the temporal resolution for high heart rates (Fig. 1). Using the available information about each sample's timing with respect to the cardiac cycle, the image reconstruction routine retrospectively computes images for any desired time in the cycle. Before the 3D inverse Fourier transform is performed to reconstruct the images, a complete set of k-space data is interpolated in the time domain for each time frame. The interpolation method used is based on the normalized convolution algorithm with a Gaussian interpolation function (22). To handle variations in heart rate during the scan, the timing is first normalized using the duration of each individual heart beat; the resulting range, from 0.0 to 1.0, describes the complete cardiac cycle (Fig. 1). Before transformation, the k-space data is zero-filled to a size of 256 × 256 × 16, giving a resulting voxel size of 1.2 × 1.2 × 8.0 mm.

Additional 2D cine gradient-echo images were acquired in long- and short-axis orientation using the following parameters: TR 25 msec, TE 10 msec, flip angle 30° (long axis) and 40° (short axis), FOV 32 cm, matrix size 256 × 128, slice thickness 7 mm, respiratory compensation used, and 16 time frames reconstructed using retrospective gating. The scan time for each slice is approximately 2 min/slice (128 heart beats for each slice). The 16 time frames are subsequently interpolated in the time domain to match the 32 time frames reconstructed for the 3D velocity data, using bilinear interpolation at each pixel.

## Phase Corrections

Two known causes of artifactual phase offsets are eddy currents and concomitant gradients. To demonstrate the effects of these phase offsets, data were obtained using a stationary phantom, using the same acquisition parameters as in the in vivo study for a single time frame.

Concomitant gradient fields are always present as soon as a magnetic field gradient is applied. These unwanted gradient fields have a non-linear spatial dependence that can be predicted from the Maxwell equations, which say that the magnetic field must have no divergence or curl. If the bipolar gradients used in phase contrast imaging are not played out simultaneously with any other gradient waveform, the effect of these concomitant fields on the resulting phase shift will cancel out. However, this will lead to an echo time that is unnecessarily prolonged, possibly causing problems with phase dispersion in complex flow. A better approach is to correct for the unwanted phase shifts in the image reconstruction process. This is possible since the correction coefficients can be calculated from a known pulse sequence (23). For each of the four velocity encoding echoes, the phase contribution from the concomitant gradient terms, $\phi_M(x,y,z)$ at each location $(x,y,z)$ is calculated according to Eq. [1] and subtracted from the acquired data.

$$\phi_M = \frac{\gamma}{2B_0} \int \left\{ (G_x^2 + G_y^2)z^2 + G_z^2 \frac{x^2 + y^2}{4} - G_x G_z xz - G_y G_z yz \right\} dt \quad [1]$$

The integral is evaluated numerically using values for the gradient waveforms $G_x(t)$, $G_y(t)$ and $G_z(t)$ corresponding to the acquisition of the center line in k-space. $B_0$ is the strength of the static magnetic field and $\gamma$ the gyromagnetic ratio.

Eddy currents cause phase shifts that can be compensated for by subtracting a linear 3D function for each velocity component (20). Each function is derived from a least-squares fit to the data from 12 areas containing stationary tissue.

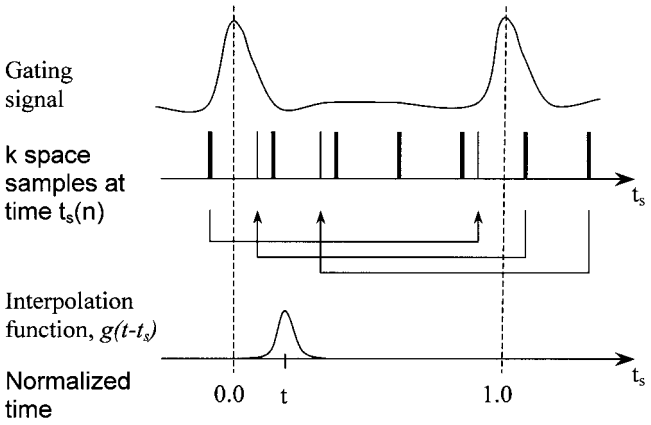


FIG. 1. Data are acquired for more than one heartbeat. Extra samples are wrapped back into the normalized heartbeat, improving the temporal resolution. A Gaussian function $g(t-t_s)$ is used for interpolation of a time frame at time t, from the samples acquired at time $t_s(n)$.

## Phase Unwrapping

Cardiac flows comprise a wide range of velocities. To describe the slow flow during the diastolic phase, a small velocity encoding range (VENC) is preferable, but this in turn causes problems with aliasing during ventricular systole. A relatively low VENC can be used if effective aliasing correction is performed. The temporal phase unwrapping technique detects and corrects aliasing based on the assumption that velocities do not change abruptly between two time frames (24). As many as 32 time frames were reconstructed from the 16 acquired k-space samples, to facilitate the use of the temporal phase unwrapping technique. As long as aliased velocity information is not present, this ensures a smooth velocity variation in time. When aliasing does occur, there is a discontinuity in the velocity time course, which is relatively easy to detect and to correct for (Fig. 2). To reduce the risk of introducing false corrections, the time course is analyzed and only voxels that have an equal number of abrupt jumps in both the negative to positive and positive to negative directions are corrected.

## Visualization

The corrected velocity data are converted to a file format that can be imported into a commercially available 3D visualization software (EnSight, CEI, Inc., Morrisville, NC). This software, which was designed for visualization of

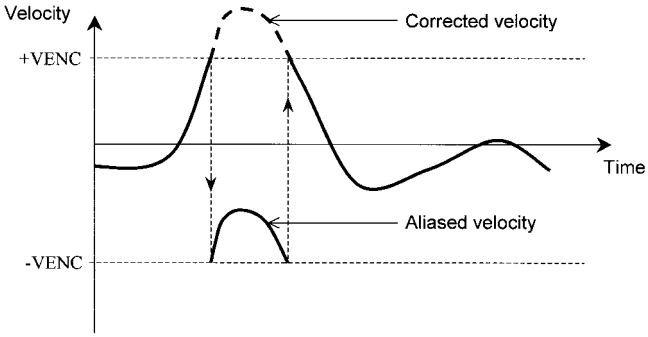


FIG. 2. The change in velocity in each voxel between consecutive time frames is analyzed to detect when aliasing occurs. Correction is only performed between pairs of positive and negative jumps (vertical arrows).

simulated data from different CFD programs, creates vector plots in any plane through the dataset, as well as streamlines, pathlines and many other kinds of flow visualization. Streamlines are based on the integration of the velocity field in a single time frame, while the pathline calculation uses the temporally resolved data and gives a realistic view of how the fluid moves as function of time. The particle traces are calculated using a fourth order Runge-Kutta numerical integration technique, which is a method that has been shown to produce an accurate particle path (25). The integration step is automatically adjusted with respect to the velocity, causing smaller steps to be taken in rapidly changing velocity fields.

In the EnSight software, an emitter grid can be positioned in the 3D data set to release particles at a desired time and location. Starting from this grid, the particles are followed for a specified time. The resulting paths can be shown either as complete traces, or in an animation mode where the particles are shown with a short tail moving along the path of the trace.

Although the software is not capable of calculating pathlines going backwards in time, this was implemented by reversing the order of the input time frames and reversing the sign of all velocity vector components.

## RESULTS

### Morphologic Visualization

The acquisition of the time-resolved 3D data set was optimized for signal strength from the blood pool, to achieve a high signal-to-noise ratio in the velocity data. These settings limit the contrast between blood and myocardium in the magnitude images, however, and impair delineation of the anatomical cardiac structures that are needed for orientation within the 3D data set. Conventional 2D cine gradient echo images were therefore also acquired in short- and long-axis views to aid in spatial orientation. Using the coordinate information given in each image file, the spatial relationship between the 2D slices and the 3D dataset was resolved and both were displayed in three dimensions in EnSight. The 3D volume containing velocity information, depicted as a white box, and five 2D slices can be seen in Fig. 3a. These give a 3D representation of the data set, which can be interactively rotated and viewed from any perspective. Since all information is acquired in a temporally resolved fashion, 2D slices and 3D velocities can also be visualized in a cine mode, adding the temporal component to the 3D visualization of both cardiac motion and flow.

### Flow Visualization

Velocity information from the 3D data set can be extracted and displayed in several different ways. A reference plane of chosen size can be placed anywhere within the 3D volume. The velocities at each point in the plane can be determined and color-coded according to a scale of velocities, as shown in Fig. 3b. The color-coding of the circular plane corresponds to speed, but the direction of the flow is not readily apparent. Displaying the velocity information as vectors shows both velocity and direction of flow, but only for selected planar regions of interest (vector plot in

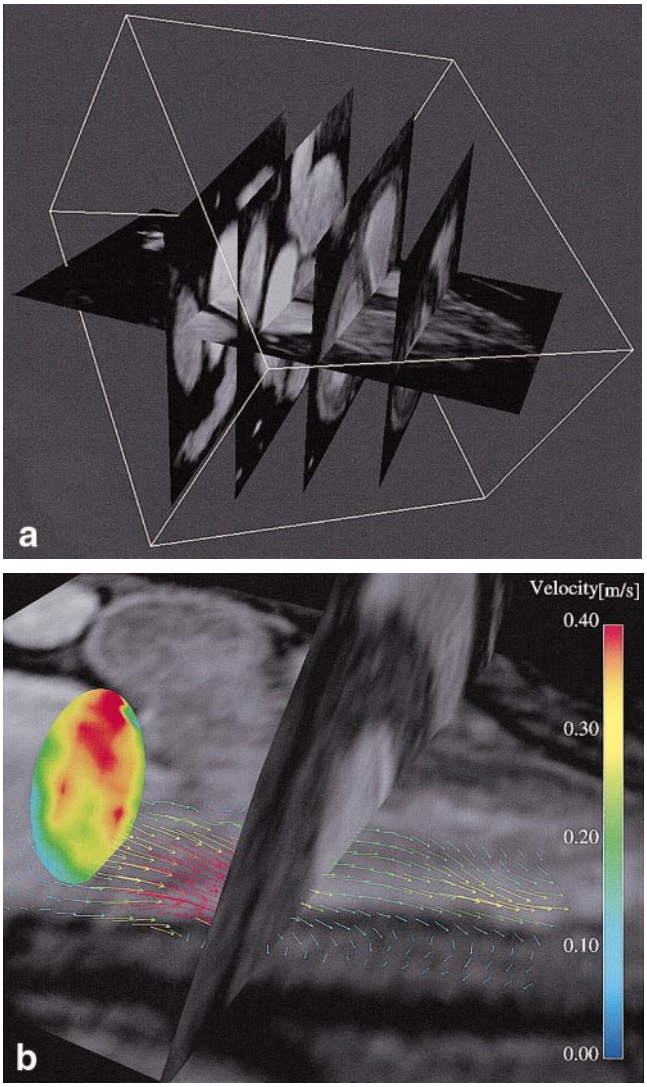


FIG. 3. **a:** Four short-axis 2D slices and one long-axis slice are shown along with the box representing the 3D velocity vector data set. **b:** Short- and long-axis 2D slices are displayed in combination with a color-coded circular plane, calculated from the 3D velocity data set . Flow directions can also be appreciated using 3D vectors from single planes, here showing the velocities in a plane parallel to the long-axis image.

Fig. 3b). A display of velocity vectors for the complete 3D region is too complex to be useful.

Pathline visualization is a much more descriptive way of displaying flow patterns and can follow them along their course anywhere within the entire 3D volume. Particle traces are constructed for the blood that crosses the reference plane at a given starting time; they follow the flow as it moves through the heart in subsequent frames. The starting time, the size and position of the reference plane, and the density of the emitted particle traces can all be defined. The flow of interest can therefore be carefully selected, and as all other concurrent velocity information is hidden, a detailed visualization of the flow path and velocities along the traces can be obtained. A typical example of pathlines, starting from the location of the mitral valve at the time of early diastolic inflow, is shown in Fig. 4. It can be readily seen how the well-organized blood moves forward from the plane into the left ventricle, makes a smooth bend near the apex, and then turns into the outflow tract. Tracing blood flow backwards in time essentially demonstrates the origin of blood flow that reaches a given location in the heart at a defined moment. This has proved very useful in locating small inflows and swirls. Backward particle traces from the same starting plane and time are also shown in Fig. 4, demonstrating the upstream left atrial flow.

The descriptive power of particle trace visualization is enhanced by animation. The length of the particle traces' ''tails,'' which represent the distance traveled during a specified time interval, can be shortened to limit the amount of information per frame and give a real-time appearance to the flow traces. The anatomical 2D slices may also be shown in cine mode in combination with the traces, creating a very realistic representation of simultaneous flow and cardiac motion. Figure 5 shows three different time frames from an animation created from the forward traces shown in Fig. 4.

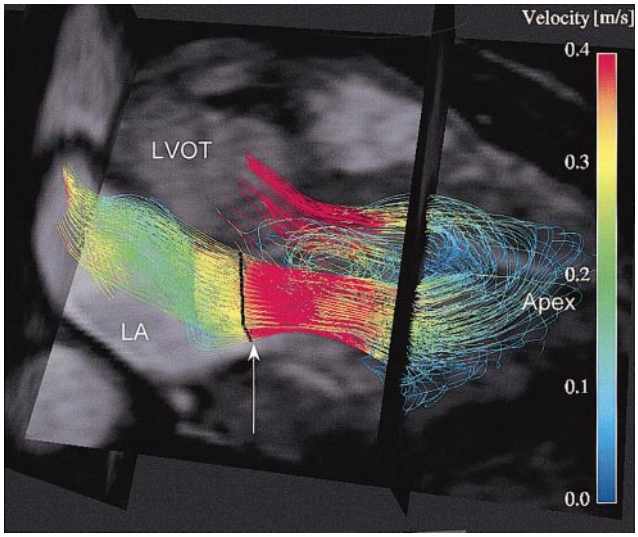


FIG. 4. Particle trace visualization of flow through a normal heart. Particles are emitted in early diastole from a plane positioned at the mitral annulus (arrow) and followed forward and backward in time. This delineates the path taken from the left atrium (LA), through the mitral valve, to the apex and out through the left ventricular outflow tract (LVOT). The traces are color coded according to velocity.

### Maxwell Corrections

The quality of the input velocity data is important for the accuracy of particle trace visualizations. Since the pathlines are calculated as the time integral of the velocity field, even a small artifactual non-zero velocity registration can create significant deviation of the pathlines, particularly if traced for a long time. The importance of these artifactual velocities is shown in particle traces calculated from the velocity data acquired from the completely stationary phantom. The theoretical particles were traced for 0.5 sec, similar to tracing times used with physiological data. This should result in traces having zero length. Figure 6a demonstrates that pathlines with significant length (more than 3 cm) are generated when the data set has only been corrected for the linear phase shifts caused by eddy currents. When the velocity data set is also corrected for the non-linear offsets caused by concomitant gradients, using the technique proposed by Bernstein et al (23), this artifactual interference is markedly reduced (Fig. 6b).

The effects of Maxwell terms on in vivo particle traces are shown in Fig. 7a. Here, the traces are calculated from data corrected for eddy currents but not for Maxwell terms. Many traces seem to pass through the myocardium due to artifactual velocity offsets. After correction also for Maxwell terms, traces from the same visualization remain appropriately within the left ventricle (Fig. 7b).

## DISCUSSION

Intracardiac flows occur in three dimensions in space and change markedly over the cardiac cycle. 2D images of these flows—while illustrative—are incomplete by definition. Our dependence on the 2D perspective may have limited the accuracy of our assessment of important flows. For example, transvalvular flows are often well understood in the immediate vicinity of the valve where mathematical solutions and in vitro modeling apply. The behavior of in vivo flows that propagate in the presence of competing, concurrent flows and changing chamber dimensions is exceptionally difficult to predict. Studies using Doppler echocardiography have detected changes in intraventricular flow in many types of valvular and myocardial disorders, but their description has been hampered by the angle sensitivity of its velocity measurements and its intrinsic 2D nature.

The 3D particle trace technique promises new observations about intracardiac flows. It has been suggested that organized vortices are important in cardiac function, and they have been detected in two dimensions using echocardiography and conventional 2D cine phase contrast techniques (4,8,26). Particle trace visualization of flow patterns based on 3D MRI data gives a more complete description of their 3D properties, unrestricted to a single imaging plane. This will improve our ability to investigate further the role of vortices in maintaining optimal cardiac flow.

Deviation from organized and efficient normal flow may be clinically important and is seen in many common cardiovascular diseases. Arrhythymias, wall motion abnor-

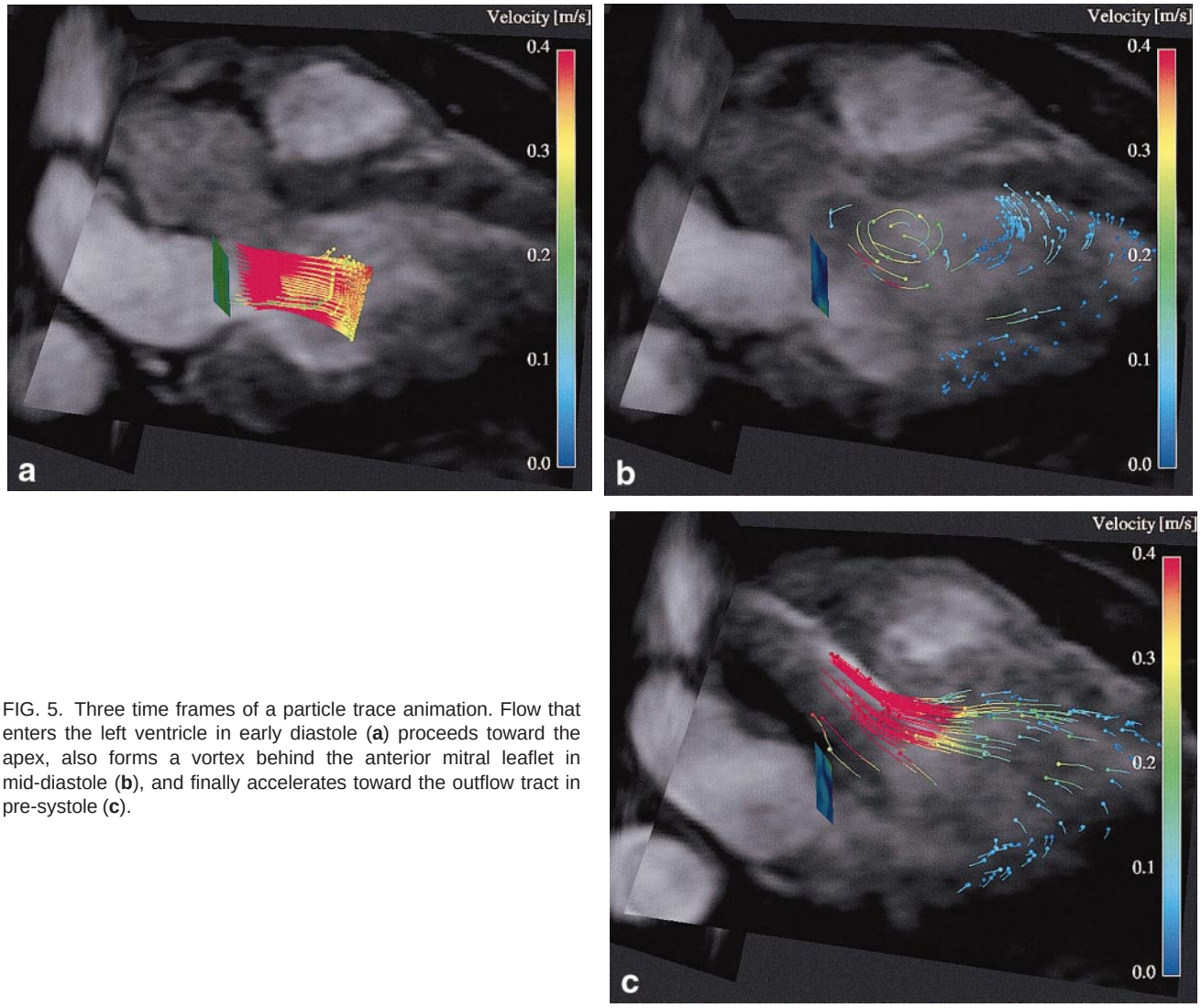


FIG. 5. Three time frames of a particle trace animation. Flow that enters the left ventricle in early diastole (**a**) proceeds toward the apex, also forms a vortex behind the anterior mitral leaflet in mid-diastole (**b**), and finally accelerates toward the outflow tract in pre-systole (**c**).

malities from ischemic heart disease, and valve replacement may all affect the normal patterns of flow (27,28) as well as increase the risks of thrombogenesis and cardiac dysfunction. If normal patterns were better understood, recognition and potential alleviation of pathologic flow abnormalities could follow. In addition, recognition of the complex in vivo patterns of valve inflow and outflow might improve prosthetic valve design and application.

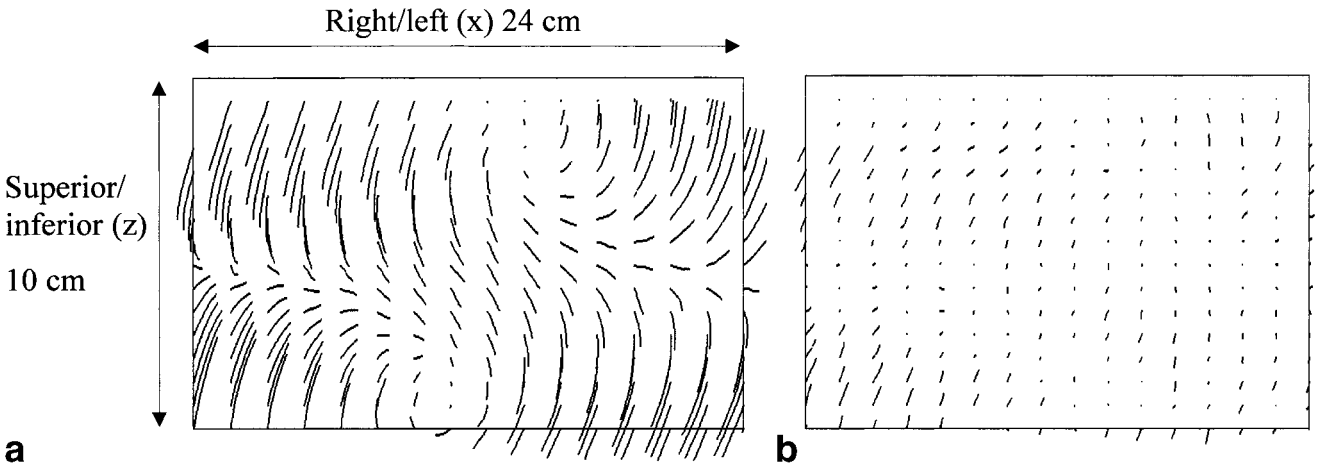


FIG. 6. Particle traces created by integration over 0.5 sec using data from a stationary phantom. **a:** Without correction for Maxwell terms, the non-zero velocities create artifactual particle traces of considerable length. **b:** Corrected data produce traces with less artifact.

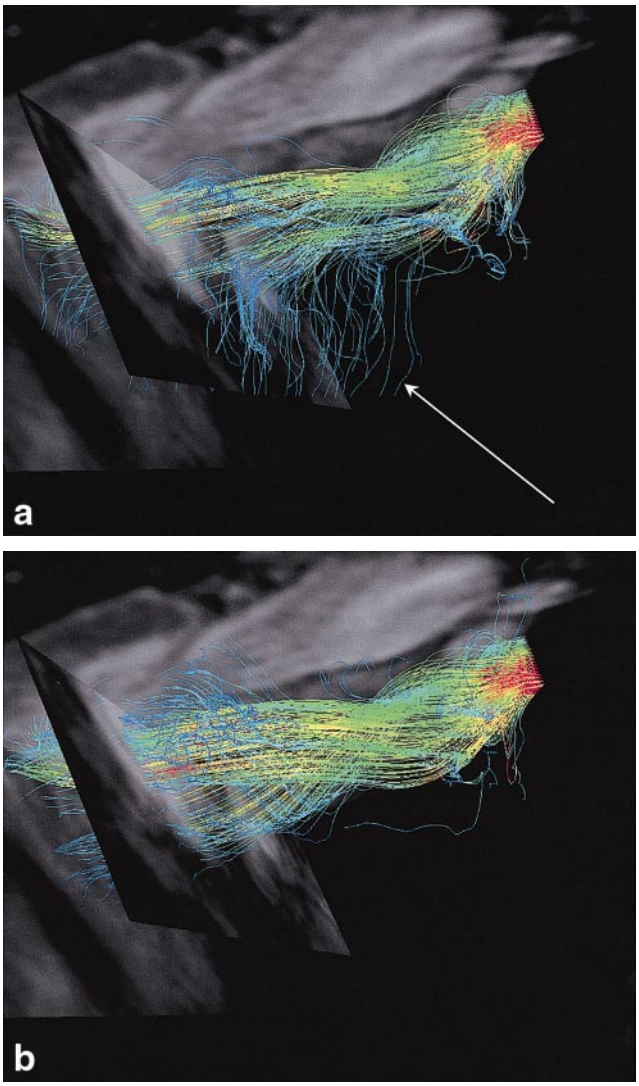


FIG. 7. **a:** Particle traces created from in vivo data not corrected for Maxwell terms. Artifactual velocities are integrated, creating several traces aberrantly leaving the heart (arrow). **b:** Using corrected data, the same calculation results in traces remaining within the confines of the cavities.

Limitations of the technique in its present stage include some blurring of the velocity data due to respiratory motion. Respiratory compensation or gating was not used in this study, to avoid prolonging the scan time. While individual images from the 3D dataset do not show severe respiratory artifacts, future improvements of the pulse sequence should aim to include respiratory compensation as well as to increase temporal and spatial resolution. Increased spatial resolution would be an advantage when studying small intracardiac vortices, while better temporal resolution would be useful when studying the timing of different events. Further optimizations of the pulse sequence, to shorten TE, TR, and subsequently the total scan time, are both desirable for patient acceptance and possible, since the current version does not use the maximum capacity available in the gradient system.

If blood flow is very unstructured or variable from beat to beat the temporal and spatial averaging of this method might introduce errors. While flow studies using other techniques do not suggest significant turbulence in the absence of valve regurgitation or prosthetic replacement (29), an improved spatial resolution would minimize the risk of signal loss due to intra-voxel phase dispersion. Convective acceleration and other higher order terms are also known to complicate phase contrast (30,31). With the use of a short TE, this should not be a serious concern in imaging the human heart except for cases of severe valve regurgitation or stenosis.

Flow pathways will be difficult to define accurately if significant intermixing of flows occurs. In that situation, particle traces might follow an artifactual admixture of flows as a result of volume averaging. To avoid misinterpretation of flow directions under mixing conditions, the motion of extremely small volumes of blood need to be followed. Studies of impedance at discrete intracardiac locations suggest, however, that streams of flow in the heart remain separated over their courses, and that intracardiac mixing does not occur to any great extent (32).

Quantitative analysis of the intracardiac particle traces will require the identification and computation of parameters describing the swirls and other rotational flow patterns observed with this technique. Temporally resolved 3D data that include information about all three velocity components facilitate a quantitative description of complex flow and avoid many of the assumptions needed with 2D methods. Other flow-related parameters, such as pressure gradients (33,34) and regional resistance (35), may also be extracted from these data and expand our assessment of dynamic intracardiac flow and energetics.

## CONCLUSIONS

3D phase contrast MRI allows particle trace pathline analysis that creates an intuitive display of complex intracardiac flow patterns. Phase unwrapping algorithms extend the usable velocity range, and phase correction minimizes important artifacts from eddy currents and concomitant magnetic fields. 3D visualization of blood flow pathways, vortices, and swirls within the human heart may represent a novel extension of our understanding of cardiac physiology. Definition of the components and behavior of normal flow may then allow investigation of the abnormal flows that accompany common cardiovascular diseases and their treatment.

## ACKNOWLEDGMENTS

The authors thank Eva Flinke for her assistance in acquiring MRI data.

## REFERENCES

1. Bellhouse BJ. Fluid mechanics of a model mitral valve and left ventricle. Cardiovasc Res 1972;6:199–210.
2. Bellhouse BJ, Talbot L. The fluid mechanics of the aortic valve. J Fluid Mech 1969;35:721–735.
3. Taylor DEM, Wade JD. The pattern of flow around the atrio-ventricular valves during diastolic ventricular filling. J Physiol 1970;207:71–72P.
4. Marinelli RA, Penney DG, Marinelli WA, Baciewicz FA. Rotary motion in the heart and blood vessels: a review. J Appl Cardiol 1991;6:421–431.

5. Beppu S, Izumi S, Miyatake K, Nagata S, Park YD, Sakakibara H, Nimura Y. Abnormal blood pathways in left ventricular cavity in acute myocardial infarction. Circulation 1988;78:157–164.
6. Garrahy PJ, Kwan OL, Booth DC, DeMaria AN. Assessment of abnormal systolic intraventricular flow patterns by Doppler imaging in patients with left ventricular dyssynergy. Circulation 1990;82:95–104.
7. Jacobs LE, Kotler MN, Parry WR. Flow patterns in dilated cardiomyopathy: a pulsed-wave and color flow Doppler study. J Am Soc Echocardiogr 1990;3:294–302.
8. Delemarre BJ, Bot H, Visser CA, Dunning AJ. Pulsed Doppler echocardiographic description of a circular flow pattern in spontaneous left ventricular contrast. J Am Soc Echocardiogr 1988;1:114–118.
9. Firmin DN, Nayler GL, Kilner PJ, Longmore DB. The application of phase shifts in NMR for flow measurement. Magn Reson Med 1990;14: 230–241.
10. Pelc NJ, Bernstein MA, Shimakawa A, Glover GH. Encoding strategies for three-direction phase-contrast MR imaging of flow. J Magn Reson Imaging 1991;1:405–413.
11. Dumoulin CL, Darrow RD, Eisner DR, Tarnawski M, Scott KT, Caro CG. Simultaneous detection of multiple components of motion with MRI. J Comput Assist Tomogr 1994;18:652–660.
12. Walker PG, Cranney GB, Scheidegger MB, Waseleski G, Pohost GM, Yoganathan AP. Semiautomated method for noise reduction and background phase error correction in MR phase velocity data. J Magn Reson Imaging 1993;3:521–530.
13. Wigström L, Sjöqvist L, Wranne B. Temporally resolved 3D phase-contrast imaging. Magn Reson Med 1996;36:800–803.
14. Bogren HG, Mohiaddin RH, Kilner PJ, Jimenez-Borreguero LJ, Yang GZ, Firmin DN. Blood flow patterns in the thoracic aorta studied with three-directional MR velocity mapping: the effects of age and coronary artery disease. J Magn Reson Imaging 1997;7:784–793.
15. Mohiaddin RH. Flow patterns in the dilated ischemic left ventricle studied by MR imaging with velocity vector mapping. J Magn Reson Imaging 1995;5:493–498.
16. Walker PG, Cranney CB, Grimes RY, Delatore J, Rectenwald J, Pohost GM, Yoganathan AP. Three-dimensional reconstruction of the flow in a human left heart by using magnetic resonance phase velocity encoding. Ann Biomed Eng 1996;24:139–147.
17. Anderson JD. Computational fluid dynamics. New York: McGraw-Hill; 1995. p 15.
18. Napel S, Lee DH, Frayne R, Rutt BK. Visualizing three-dimensional flow with simulated streamlines and three-dimensional phase-contrast MR imaging. J Magn Reson Imaging 1992;2:143–153.
19. Buonocore MH. Algorithms for improving calculated streamlines in 3-D phase contrast angiography. Magn Reson Med 1994;31:22–30.
20. Pelc NJ, Herfkens RJ, Shimakawa A, Enzmann DR. Phase contrast cine magnetic resonance imaging. Magn Reson Q 1991;7:229–254.
21. Spraggins TA. Wireless retrospective gating: application to cine cardiac imaging. Magn Reson Imaging 1990;8:675–681.
22. Knutsson H, Westin CF. Normalized and differential convolution: methods for interpolation and filtering of incomplete and uncertain data. In: Proceedings of the IEEE Computer Society Conference on Computer Vision and Pattern Recognition, New York, 1993. p 515–523.
23. Bernstein MA, Zhou XJ, Polzin JA, King KF, Ganin A, Pelc NJ, Glover GH. Concomitant gradient terms in phase contrast MR: analysis and correction. Magn Reson Med 1998;39:300–308.
24. Xiang QS. Temporal phase unwrapping for CINE velocity imaging. J Magn Reson Imaging 1995;5:529–534.
25. Darmofal DL, Haimes R. An analysis of 3D particle path integration algorithms. J Comput Physics 1996;123:182–195.
26. Kim WY, Walker PG, Pedersen EM, Poulsen JK, Oyre S, Houlind K, Yoganathan AP. Left ventricular blood flow patterns in normal subjects: a quantitative analysis by three-dimensional magnetic resonance velocity mapping. J Am Coll Cardiol 1995;26:224–238.
27. Pop G, Sutherland GR, Roelandt J, Vletter W, Bos E. What is the ideal orientation of a mitral disc prosthesis? An in vivo haemodynamic study based on colour flow imaging and continuous wave Doppler. Eur Heart J 1989;10:346–353.
28. Jones M, Eidbo EE. Doppler color flow evaluation of prosthetic mitral valves: experimental epicardial studies. J Am Coll Cardiol 1989;13:234–240.
29. Bluestein D, Einav S. Transition to turbulence in pulsatile flow through heart valves—a modified stability approach. J Biomech Eng 1994;116: 477–487.
30. Oshinski JN, Ku DN, Bohning DE, Pettigrew RI. Effects of acceleration on the accuracy of MR phase velocity measurements. J Magn Reson Imaging 1992;2:665–670.
31. Steinman DA, Ethier CR, Rutt BK. Combined analysis of spatial and velocity displacement artifacts in phase contrast measurements of complex flows. J Magn Reson Imaging 1997;7:339–346.
32. Irisawa H, Wilson MF, Rushmer RF. Left ventricle as a mixing chamber. Circ Res 1960;8:183–187.
33. Greenberg NL, Vandervoort PM, Thomas JD. Instantaneous diastolic transmitral pressure differences from color Doppler M mode echocardiography. Am J Physiol 1996;271:H1267–H1276.
34. Yang GZ, Kilner PJ, Wood NB, Underwood SR, Firmin DN. Computation of flow pressure fields from magnetic resonance velocity mapping. Magn Reson Med 1996;36:520–526.
35. Voelker W, Reul H, Nienhaus G, Stelzer T, Schmitz B, Steegers A, Karsch KR. Comparison of valvular resistance, stroke work loss, and Gorlin valve area for quantification of aortic stenosis. Circulation 1995;91:1196–1204.